Energetic particle irradiation study of TiN coatings: are these films appropriate for accident tolerant fuels?

Matheus A. Tunes[a,], Felipe C. da Silva[b], Osmane Camara[a], Claudio G. Schön[b], Julio C. Sagas[c], Luis C. Fontana[c], Stephen E. Donnelly[a], Graeme Greaves[a], Philip D. Edmondson[d]

[a]*School of Computing and Engineering, University of Huddersfield, Queensgate, HD1 3DH, United Kingdom.*
[b]*Department of Metallurgical and Materials Engineering, Escola Politécnica da Universidade de São Paulo, Av. Prof. Mello Moraes, 2463, 05508-900 São Paulo-SP, Brazil.*
[c]*Laboratory of Plasmas, Films and Surfaces, Universidade do Estado de Santa Catarina, Rua Paulo Malschitzki, 200 – Zona Industrial Norte, 89219-710, Joinville-SC, Brazil.*
[d]*Materials Science and Technology Division, Oak Ridge National Laboratory, Oak Ridge TN, 37831, United States of America.*

Abstract

Coating nuclear fuel cladding alloys with hard thin films has been considered as an innovative solution to increase the safety of nuclear reactors, in particular during a of loss-of-coolant accident (LOCA). In this context, and due to its suitable mechanical properties and high corrosion resistance, titanium nitride thin films have been proposed as candidate coatings for zirconium alloys in new accident tolerant fuels for light water reactors. Although the properties of TiN hard coatings are known to be adequate for such applications, the understanding of how the exposure to energetic particle irradiation changes the microstructure and properties of these thin films is still not fully understood. Herein, we report on heavy ion irradiation *in situ* within a Transmission Electron Microscopy of magnetron-sputtered TiN thin films. The coatings were irradiated with 134 keV Xe^+ ions at 473K to a fluence of $6.7{\times}10^{15}$ ions·cm^{-2} corresponding to 6.2 displacements-per-atom where significative microstructural alterations have been observed. Post-irradiation analytic characterisation with Energy Filtered TEM and Energy Dispersive X-ray spectroscopy carried out in a Scanning Transmission Electron Microscope indicates that TiN thin films are subjected to Radiation Induced Segregation. Additionally, the nucleation and growth of Xe bubbles appears to play a major role in the dissociation of the TiN thin film.

Keywords: Thin Films, Titanium Nitride, Ion irradiation with *in situ* TEM, Accident Tolerant Fuels, Radiation Damage

1. Introduction

The Fukushima-Daiichi nuclear accident in 2011 has established new challenges for research and development towards the consolidation of Accident Tolerant Fuels (ATF) [1, 2]. Zirconium is currently the major constituent of fuel assembly alloys used in the nuclear industry worldwide; however,

Email address: m.a.tunes@hud.ac.uk (Matheus A. Tunes)

at high temperatures and during LOCA events, these alloys suffer from oxidation by steam which increases the hydrogen gas generation rate [3–6]. This dangerous accumulation of hydrogen gas could be mitigated or even avoided if the zirconium-based alloys were coated with a protective thin film.

Among the variety of commercially available thin films that could serve this purpose, titanium nitride (TiN) is widely used in several industries such as mechanical tools, medical implants and aerospace engineering [7]. TiN thin films have recently been proposed as hard coatings for zirconium-based alloys in Light-Water Reactors (LWRs) [8, 9] mainly due to their desirable properties of high mechanical strength [10], suitable corrosion resistance [11] and tribological behaviour [12]. However, with prolonged exposure to the extreme environment of a nuclear reactor these properties will be modified (often degraded) [13]. Therefore, it is important to evaluate the performance of these candidate materials when exposed to displacing irradiation, prior to their use in reactors.

To date, the radiation resistance of TiN thin films has been studied in a wide variety of conditions. The microstructure of polycrystalline TiN thin films was studied at room temperature and under light ion irradiation by Wang *et al.* and Wan *et al.* up to fluences of 1×10^{17} ions·cm^{-2}. These authors observed that the grain boundaries, which are abundant in nanocrystals, acted as sinks for radiation-induced Frenkel pairs, providing pathways for diffusion and annihilation, thus suggesting a certain degree of radiation tolerance [14, 15]. The radiation performance of TiN films under Ar ion irradiation at room temperature has also been studied by Popovic *et al.* [16]. These authors observed that the 120 keV Ar irradiation caused a decrease of the lattice parameter of TiN crystals from 0.427 to 0.423 nm which resulted in an increase of the strain in the film layer at fluences of 1×10^{16} ions·cm^{-2}. At higher fluences, 2×10^{17} ions·cm^{-2} and higher irradiation energies, 200 keV Ar^{+}, the increase of the electrical resistivity of the irradiated TiN thin films was attributed to the formation of smaller grains as a result of the ion collisions with the film microstructure [17]. In a later work the same authors carried out irradiation with heavy ions – 400 keV Xe up to 2×10^{16} ions·cm^{-2} at room temperature – and observed that in the irradiated film, XRD measurements exhibited the split of the (111) reflection which indicated both phase transformations as well as contraction of the TiN lattice [18] as opposed to Xue *et al.* who observed expansion of the TiN lattice under 100 keV Ar irradiation at 873 K [19]. Uglov *et al.* reported that small Zr additions into the TiN may increase its structural stability under heavy ion irradiation [20], but no post-irradiation microstructural analysis was performed by the authors.

The different microstructural changes induced by ion irradiation in TiN thin films suggested that this material is strongly sensitive to the conditions of the experiment such as fluence, temperature and ion species, therefore an *in situ* TEM ion irradiation study could probe whether such TiN thin films can be regarded as a good candidate for hard coatings in the nuclear industry, while also revealing possible mechanisms of degradation. We report in the present work a heavy ion irradiation study *in situ* within a TEM that assesses the microstructural evolution of the TiN thin films as a function of the irradiation dose. The thin films were irradiated at 473 K and the post-irradiation characterisation has been performed using the analytical techniques of Energy-Filtered TEM (EFTEM) and Energy-Dispersive X-ray Spectroscopy (EDX) within a Scanning Transmission Electron Microscope (STEM). The observation of radiation damage in real time at the nanoscale of the TiN thin films reported in this work, has led to an improved understanding of the radiation damage mechanisms at the fundamental level.

2. Materials and Methods

2.1. Synthesis of the TiN thin films

TiN thin films were deposited on Al-Si alloy substrates by the DC grid-assisted magnetron sputtering (GAMS) technique in an Ar+N_2 discharge. This technique is described further elsewhere [21–23]. The substrate was polished and ultrasonically cleaned in tetrachloroethylene for 10 minutes prior to deposition. The system's chamber was then pumped down to a base pressure of 10^{-2} Pa and the substrate temperature was held at 573 K throughout the deposition. The 99.5% pure Ti target was sputtered prior to deposition to remove any oxide or surface contamination. The grid was grounded and placed 20 mm from the target. The substrate distance from the sputtering target was 60 mm. The deposition was performed at a working pressure of 0.40 Pa with a discharge current of 2.00 A. A DC bias of -30 V was applied to the substrate. The total deposition time was 30 min and the N_2 flow was fixed at 7.7 sccm. The deposition rate was around of 65 nm·min^{-1}. A Ti interlayer was deposited during 2 minutes, in order to improve TiN film adhesion. After deposition, the thickness of the deposited thin films were measured cross-sectionally in the FIB to be around of 1.5–2 μm.

2.2. Focused Ion Beam

In order to produce electron-transparent lamellae from the deposited TiN thin film, the conventional focused-ion beam (FIB) technique for TEM sample preparation was used, and a top protection

layer of Pt with a thickness of 2.0 μm was deposited onto the thin film surface to reduce FIB damage/gallium contamination (as recommended by [24, 25]).

2.3. In situ TEM with heavy ion irradiation

The *in situ* TEM with heavy ion irradiation was carried out at the MIAMI facility using the MIAMI-2 system with 134 keV Xe^{+} ions at 473 K with a flux of 1.6×10^{13} ions·cm^{-2}·s^{-1}. Considering that TiN has a melting point higher than 3200 K[26], the irradiation was performed at a homologous temperature of around $0.15T_m$ which is close to the primary inlet (coolant) temperature of most LWRs. Additionally, this temperature was chosen in order to minimise bulk diffusion. The microstructural evolution of the TiN thin film was monitored during irradiation with a Hitachi H9500 Transmission Electron Microscope operating at 300 keV and images were recorded using a Gatan OneView digital camera with 16 Mpx.

2.4. Monte Carlo calculations and fluence-to-dpa conversion

Fluence-to-dpa conversions were performed using the Monte Carlo code Stopping and Range of Ions in Matter (SRIM) outputs [27] and a mathematical procedure suggested by Stoller et al. [28]. The thickness of the thin film lamellae was assumed to be 100 nm. Additional parameters used in the conversion were the TiN density of 5.4 g·cm^{-3} and its atomic density of 1.058×10^{23} atoms·cm^{-3} [29]. In this work the thin films were irradiated up to a fluence of 6.7×10^{15} ions·cm^{-2} corresponding to 6.2 dpa. Due to the observed microstructural alterations in the damaged microstructure of the thin films, the irradiations were stopped at 6.2 dpa aiming at further post-irradiation characterisation.

2.5. Post-irradiation characterisation

Post-irradiation analysis was performed using a Gatan GIF Quantum SE camera model 693 for Energy Filtered Transmission Electron Microscopy (EFTEM) in the Hitachi H9500 TEM at the MIAMI-2 Facility and with a FEI Talos F200X Scanning Transmission Electron Microscope operating at 200 keV for Energy Dispersive X-ray (EDX) mapping located at the Low-Activation Materials Development and Analysis (LAMDA) Laboratory at the Oak Ridge National Laboratory. This instrument combines high-resolution scanning/transmission electron microscope imaging with a large solid angle (0.9 srad) windowless EDX detector. The post-irradiation EDX mapping taken with the FEI Talos allowed Multivariate Statistical Analysis (MVSA) [30] to be performed. The software ImageJ [31]

was used to measure the size of the Xe bubbles from the micrographs following a procedure described elsewhere [32].

3. Results

The pristine microstructure of the magnetron-sputtered TiN thin films consisted of small grains with sizes from 20 to 100 nm as exhibited in the bright-field TEM (BFTEM) micrograph 1(a). During the irradiation, Xe bubbles were observed to form in the microstructure of the TiN at fluences of around 9.5×10^{14} ions·cm^{-2} (0.9 dpa). At doses of around 2.9×10^{15} ions·cm^{-2} (2.6 dpa), the grain boundaries of these nanocrystals were observed to exhibit darker diffraction contrast following the observation of Xe bubbles with an average diameter of 4.1±2.2 nm as shown in the BFTEM micrograph 1(b). At the end of the experiment with a dose of around 6.7×10^{15} ions·cm^{-2} (6.2 dpa), the Xe bubbles had grown to an average diameter of 25.2±4.8 nm and the TiN grain boundaries were clearly darker as exhibited in micrograph 1(c). Using the software ImageJ, it was possible to measure the diameter distribution of Xe bubbles at 2.6 and 6.2 dpa as exhibited in figure 2.

The insets in the micrographs 1(i) and 1(iii) are diffraction patterns (DPs) that were taken before and after irradiation using the selected area diffraction (SAD) aperture on the same area of interest. The DP before irradiation confirms the nanocrystalline nature of the TiN grains. After irradiation, the DP shows that the TiN has not amorphised under these irradiation conditions and also exhibit smaller grains indicating grain refinement.

Post-irradiation characterisation with EFTEM has revealed that at 6.2 dpa, Ti segregated to the grain boundaries. These EFTEM results were validated with higher resolution EDX mapping in the STEM as shown in the set of micrographs in figure 3. The EDX mapping also shows that Ti has accumulated within the Xe bubbles positions. By means of the multivariate statistical analysis (figure 4), the identification of a phase with strong Ti and Xe signals confirms the association of Xe bubbles with segregated Ti atoms.

4. Discussion

Under heavy-ion irradiation the grain boundaries of the TiN nanocrystals exhibited significant changes with increasing irradiation dose.

During irradiation the grain boundaries became darker which has been identified as a change in mass-thickness of the nanocrystals, caused by the presence of heavier elements at the grain bound-

aries. On the analytical characterisation side both EFTEM and STEM-EDX techniques have detected the segregation of Ti preferentially at the grain boundaries. These microstructural differences from pristine to 6.2 dpa in combination with the detection of Ti along the grain boundaries show that the TiN thin film was subjected to the radiation-induced segregation (RIS) phenomenon. The observed growth of Xe bubbles upon increasing the irradiation dose suggests a correlation of RIS with the nucleation of inert gas bubbles.

RIS can be described as irradiation-assisted diffusion promoted by the atomic collisions when materials are exposed to energetic particle bombardment. In the context of nuclear reactor technology, RIS has already been associated with accelerating material degradation mechanisms such as thermal ageing [33, 34] and stress corrosion cracking [35]. The preferential migration of Ti towards grain boundaries, as reported in this work at around a dose of 2.9×10^{15} ions·cm^{-2} (2.6 dpa), suggests that the interfaces of the TiN nanocrystals are acting as sinks for irradiation-induced defects. Such Ti segregation increases with dose (6.2 dpa) thus confirming that irradiation plays a major role when TiN thin films are subjected to radiation damage.

The collision cascade generated upon the impact of an energetic Xe ion with the TiN generates a profile of recoil atoms with cascade diameters as large as 30 nm (figure 5): which is of the order of the thin film grain size. The shape of the collision cascade can be used to shed light on the RIS phenomenon: although a great portion of these defects will recombine and readily annihilate [36], upon increasing the irradiation dose, successive accumulation, displacement and replacement of recoiled atoms will generate a flux of Ti and N atoms towards the grain boundaries which is also affected by the nucleation and growth of inert gas bubbles.

A particular consideration regarding the damaged microstructure of the TiN thin film is the growth of Xe bubbles. The Xe atom is known to have reduced mobility in ceramic-based materials at low homologous temperatures [37]: the irradiation in this work was carried out at $\approx 0.15 T_m$. However, the Xe bubbles were observed to grow around 600% from 2.6 dpa to 6.2 dpa as shown in the histograms of size distributions in figure 2. An explanation for this accelerated growth may be related to the RIS phenomenon and the nanocrystalline nature of the deposited TiN thin films.

Inert gas bubbles grow upon the arrival of vacancies [36, 38]. Once a bubble nucleates, the atoms of the material have to be accommodated somewhere in the microstructure. At lower doses and given the accelerated atomic diffusion by RIS, a possible home for the migration of displaced Ti atoms is

the grain boundaries as confirmed by both EFTEM and STEM-EDX. But at higher doses (> 6 dpa), the large inert gas bubbles also begin to act as sinks for segregated atoms. This has been confirmed by the MVSA as shown in figure 4. An X-ray peak corresponding to Ti has been detected in the positions where Xe bubbles were observed. A schematic model for the mechanisms herein described is showed in figure 6.

An additional factor is related to the role of nitrogen in the process. Nitrogen present in the TiN structure is also displaced by the heavy ion bombardment. Eventually displaced monoatomic N will reach the site of an existing bubble, either as a result of the direct bombardment or as result of diffusion. Monoatomic N is a highly reactive species. As our results show, the bubbles can be enriched in Ti, therefore some of these atoms will recombine with this excess of Ti, but a fraction will survive long enough to meet another monoatomic N atom, thus allowing the formation of molecular nitrogen which is a stable compound. This may also diffuse into a bubble, increasing the gas uptake by the bubble, leading to an enhanced growth rate for the bubble. The lack of N signal at the site of the bubbles can be justified by the relatively small atomic number of N (compared, for example, to Xe), which impairs detection using spectroscopic methods. Another fact for consideration may be the absorption of the soft N K_α X-ray, thus contributing to its attenuation during the STEM-EDX measurements. These mechanisms are likely to be observed in any material containing species prone to form gaseous compounds (*e.g.* systems containing C and N (leading to CN) or C and O (leading to CO).

Some considerations regarding the possible applicability of TiN thin films as hard coatings for ATF systems within the nuclear technology have to be addressed. The grain boundaries of TiN thin films were identified by Wang *et al.* as potential annihilation regions for the recombination of radiation-induced defects and this fact has led authors [14] to conclude that TiN hard coatings are potentially radiation resistant. Similar results were obtained with ion irradiation by other authors [16–19, 39]. The present work has shown that, in fact, the grain boundaries have Ti-enrichment and also indicates that after the nucleation of inert gas bubbles, the kinetics of Ti segregation can be accelerated. The detection of Ti segregation suggests that the TiN suffers dissociation under energetic particle bombardment. Although Xe is not a product of the decay chains of either Ti or N, nuclear transport calculations showed that inside a nuclear reactor, N transmutation reactions produce He at a rate around of 318 appm per year (and also H at arate of 8277 appm per year) [40]. As ATF systems

are expected to operate up to high doses (between 200-500 dpa [13]), the production of He under transmutation of N atoms will lead to the nucleation of inert gas bubbles that could contribute to the Ti segregation as observed in this work for Xe bubbles.

The nucleation and growth of inert gas bubbles also introduces additional complications for the application of TiN within the context of ATF systems and safer nuclear reactors. The regions around bubbles and voids can significantly increase the stress concentration factor, leading to the formation of cracks under the application of external load [41]. As well as the formation of cracks, inert gas bubbles will also contribute to the embrittlement of the TiN microstructure that will reduce the ability to mechanically deform, which is already limited for hard coatings [42]. It may also result in swelling which would pose a significant problem for removal of fuel assemblies. The combination of inert gas bubble nucleation and growth with Ti segregation preferentially along the grain boundaries suggested that the microstructures exhibited in figure 1(c) are a characteristic of swollen nanocrystals.

$$Ti(s) + 2H_2O(g) \longrightarrow TiO_2(s) + 2H_2(g) \tag{1}$$

A final topic remains to be addressed. As reported here, TiN nanocrystals are subjected to dissociation under exposure to energetic particle irradiation. After irradiation, Ti-enriched zones are created which will experience the same oxidation reaction as Zr-based alloys [5] (equation 1) in the environment of a nuclear reactor at high temperatures during LOCA events and will also contribute to an increased generation rate of hydrogen gas: a factor that needs to be reduced in the context of ATF systems.

5. Conclusion

In this work, the microstructure of titanium nitride thin films under heavy ion irradiation using *in situ* TEM was investigated. The nucleation and growth of Xe bubbles was correlated with the TiN dissociation and segregation into two preferential sites: (i) along the grain boundaries of the nanocrystals and (ii) within the Xe bubbles. The local morphological alterations in the microstructure of the TiN identified by *in situ* TEM suggest that TiN thin films can experience radiation-induced segregation under displacing irradiation. It has also been observed that upon growth, the inert gas bubbles can contribute to an enhancement of the RIS effect.

The results reported here show that nanocrystalline TiN thin films may not be a suitable solution

for coating Zr-based alloys in future accident tolerant fuels systems mainly because the TiN is prone to dissociate under energetic particle bombardment, creating Ti-enriched zones in which oxidation at high temperatures will generate hydrogen gas in a similar way to that for Zr-alloys under accident conditions. If hard thin films are to be applied to new ATF systems, the results in this paper suggest that materials with reduced activation – to avoid formation of inert gas bubbles from nuclear reactions (*e.g.* (n,α)) – are particularly preferred.

In order to reduce or possibly suppress the RIS effect, MAX Phases [43] and High-Entropy Alloys [44, 45] should be taken into consideration for future radiation damage and tribology studies on coating Zr-based alloys for the nuclear industry. The intense recent research on these materials have indicated a potential high phase stability under energetic particle bombardment when compared with conventional ceramic materials and metallic alloys, and this could imply – from a microstructural perspective – a superior tolerance against the multiple deleterious effects of energetic particle irradiation [43, 45].

6. Acknowledgements

MAT was supported through the ASTRO fellowship, a United States Department of Energy workforce development program implemented at Oak Ridge National Laboratory through the Oak Ridge Institute for Science and Education under contract DE-AC05-06OR23100. CGS acknowledges the financial support by the São Paulo state research funding agency (FAPESP, São Paulo, Brazil), under grant 2016/25248-3. LCF and JCS acknowledge the financial support by the Santa Catarina state research funding agency (FAPESC, Santa Catarina, Brazil) through the program PAP in association with the Santa Catarina State University under contract PAP-TR 655. This research was performed, in part, using instrumentation (FEI Talos) provided by the Department of Energy, Office of Nuclear Energy, Fuel Cycle R&D Program and the Nuclear Science User Facilities under grant number NAE278. The authors are grateful to the Engineering and Physical Sciences Research Council (EPRSC) for funding the MIAMI facilities (grants numbers EP/E017266/1 and EP/M028283/1). MAT, GG and OC would like thank Benjamin Clay (University of Huddersfield) for useful discussions on radiation damage calculations.

7. Data Availability

The raw/processed data and the experimental parameters are available to download from Mendeley Data by using the identifier doi:10.17632/54rygzkzkh.2 link.

8. References

References

[1] M. Kurata, Research and development methodology for practical use of accident tolerant fuel in light water reactors, Nuclear Engineering and Technology 48 (1) (2016) 26–32.

[2] K. Terrani, Accident tolerant fuel cladding development: Promise, status, and challenges, Journal of Nuclear Materials 501 (2018) 13–30.

[3] F. Tanabe, Analyses of core melt and re-melt in the fukushima daiichi nuclear reactors: Fukushima npp accident related, Journal of Nuclear Science and Technology 49 (1) (2012) 18–36.

[4] M. A. Tunes, R. W. Harrison, G. Greaves, J. Hinks, S. Donnelly, Effect of he implantation on the microstructure of zircaloy-4 studied using in situ tem, Journal of Nuclear Materials 493 (2017) 230–238.

[5] R. Pawel, J. Cathcart, R. McKee, The kinetics of oxidation of zircaloy-4 in steam at high temperatures, Journal of the Electrochemical Society 126 (7) (1979) 1105–1111.

[6] M. A. Tunes, C. M. Silva, P. D. Edmondson, Site specific dependencies of hydrogen concentrations in zirconium hydrides, Scripta Materialia 158 (2019) 136 – 140.

[7] W. D. Sproul, Physical vapor deposition tool coatings, Surface and Coatings Technology 81 (1) (1996) 1–7.

[8] E. Alat, A. T. Motta, R. J. Comstock, J. M. Partezana, D. E. Wolfe, Ceramic coating for corrosion (c3) resistance of nuclear fuel cladding, Surface and Coatings Technology 281 (2015) 133–143.

[9] E. Alat, A. T. Motta, R. J. Comstock, J. M. Partezana, D. E. Wolfe, Multilayer (tin, tialn) ceramic coatings for nuclear fuel cladding, Journal of Nuclear Materials 478 (2016) 236 – 244.

[10] S. Vepřek, S. Reiprich, A concept for the design of novel superhard coatings, Thin solid films 268 (1-2) (1995) 64–71.

[11] D. Starosvetsky, I. Gotman, Corrosion behavior of titanium nitride coated ni–ti shape memory surgical alloy, Biomaterials 22 (13) (2001) 1853–1859.

[12] Y. Y. Guu, J. F. Lin, C.-F. Ai, The tribological characteristics of titanium nitride, titanium carbonitride and titanium carbide coatings, Thin solid films 302 (1-2) (1997) 193–200.

[13] S. J. Zinkle, G. Was, Materials challenges in nuclear energy, Acta Materialia 61 (3) (2013) 735–758.

[14] H. Wang, R. Araujo, J. Swadener, Y. Wang, X. Zhang, E. Fu, T. Cagin, Ion irradiation effects in nanocrystalline tin coatings, Nuclear Instruments and Methods in Physics Research Section B: Beam Interactions with Materials and Atoms 261 (1-2) (2007) 1162–1166.

[15] Q. Wan, B. Yang, H. Liu, Q. Mei, Y. Chen, Ion irradiation tolerance of tisin nanocomposite coating, Surface and Coatings Technology 305 (2016) 165–169.

[16] M. Popović, M. Novaković, N. Bibić, Structural characterization of tin coatings on si substrates irradiated with ar ions, Materials characterization 60 (12) (2009) 1463–1470.

[17] M. Popović, M. Novaković, A. Traverse, K. Zhang, N. Bibić, H. Hofsäss, K. Lieb, Modifications of reactively sputtered titanium nitride films by argon and vanadium ion implantation: Microstructural and opto-electric properties, Thin Solid Films 531 (2013) 189–196.

[18] M. Popović, M. Novaković, M. Mitrić, K. Zhang, Z. Rakočević, N. Bibić, Xenon implantation effects on the structural and optical properties of reactively sputtered titanium nitride thin films, Materials Research Bulletin 91 (2017) 36–41.

[19] J.-X. Xue, G.-J. Zhang, F.-F. Xu, H.-B. Zhang, X.-G. Wang, S.-M. Peng, X.-G. Long, Lattice expansion and microstructure evaluation of ar ion-irradiated titanium nitride, Nuclear Instruments and Methods in Physics Research Section B: Beam Interactions with Materials and Atoms 308 (2013) 62–67.

[20] V. V. Uglov, D. P. Rusalski, S. V. Zlotski, A. V. Sevriuk, G. Abadias, S. B. Kislitsin, K. K. Kadyrzhanov, I. D. Gorlachev, S. N. Dub, Stability of Ti-Zr-N coatings under Xe-ion irradiation, Surface and Coatings Technology 204 (12-13) (2010) 2095–2098.

[21] J. C. Sagás, D. A. Duarte, D. R. Irala, L. C. Fontana, T. R. Rosa, Modeling reactive sputter deposition of titanium nitride in a triode magnetron sputtering system, Surface and Coatings Technology 206 (2011) 1765–1770.

[22] J. C. Sagás, L. C. Fontana, H. S. Maciel, Influence of electromagnetic confinement on the characteristics of a triode magnetron sputtering system, Vacuum 85 (2011) 705–710.

[23] L. C. Fontana, J. L. R. Muzart, Triode magnetron sputtering tin film deposition, Surface and Coatings Technology 114 (1) (1999) 7–12.

[24] J. Li, T. Malis, S. Dionne, Recent advances in FIB and TEM specimen preparation techniques, Materials Characterization 57 (1) (2006) 64–70.

[25] L. Giannuzzi, F. Stevie, A review of focused ion beam milling techniques for TEM specimen preparation, Micron 30 (3) (1999) 197–204.

[26] P. Broz, G. Rogl, X. Yan, M. Premović, V. Soprunyuk, P. Heirich, E. Bauer, W. Schranz, P. Rogl, Physical properties of $TiMn_2$ and interaction with refractory TiN (system Ti – Mn – N), J. Alloys Comp. 740 (2018) 647 – 659.

[27] J. F. Ziegler, M. D. Ziegler, J. P. Biersack, Srim–the stopping and range of ions in matter (2010), Nuclear Instruments and Methods in Physics Research Section B: Beam Interactions with Materials and Atoms 268 (11-12) (2010) 1818–1823.

[28] R. E. Stoller, M. B. Toloczko, G. S. Was, A. G. Certain, S. Dwaraknath, F. A. Garner, On the use of SRIM for computing radiation damage exposure, Nuclear Instruments and Methods in Physics Research Section B: Beam Interactions with Materials and Atoms 310 (2013) 75–80.

[29] H. O. Pierson, Handbook of refractory carbides and nitrides: properties, characteristics, processing and applications, William Andrew, 1996.

[30] C. M. Parish, L. N. Brewer, Multivariate statistics applications in phase analysis of stem-eds spectrum images, Ultramicroscopy 110 (2) (2010) 134–143.

[31] C. A. Schneider, W. S. Rasband, K. W. Eliceiri, Nih image to imagej: 25 years of image analysis, Nature methods

9 (7) (2012) 671.

[32] R. W. Harrison, G. Greaves, J. Hinks, S. Donnelly, Engineering self-organising helium bubble lattices in tungsten, Scientific reports 7 (1) (2017) 7724.

[33] D. R. Arkell, P. C. L. Pfeil, Transmission electron microscopical examination of irradiated austenitic steel tensile specimens, Journal of Nuclear Materials 12 (2) (1964) 145–152.

[34] H. Wiedersich, P. R. Okamoto, N. Q. Lam, A theory of radiation-induced segregation in concentrated alloys, Journal of Nuclear Materials 83 (1) (1979) 98–108.

[35] J. Busby, G. Was, E. Kenik, Isolating the effect of radiation-induced segregation in irradiation-assisted stress corrosion cracking of austenitic stainless steels, Journal of Nuclear Materials 302 (1) (2002) 20–40.

[36] M. W. Thompson, Defects and Radiation Damage in Metals, Defects and Radiation Damage in Metals, by M. W. Thompson, Cambridge, UK: Cambridge University Press, 1974.

[37] D. L. Morrison, T. S. Elleman, D. N. Sunderman, Diffusion of xenon in ceramic oxides, Journal of Applied Physics 35 (5) (1964) 1616–1622.

[38] S. E. Donnelly, The density and pressure of helium in bubbles in implanted metals: A critical review, Radiation Effects 90 (1-2) (1985) 1–47.

[39] M. Popović, M. Novaković, Z. Rakočević, N. Bibić, Tailoring the structural and optical properties of tin thin films by ag ion implantation, Nuclear Instruments and Methods in Physics Research Section B: Beam Interactions with Materials and Atoms 389 (2016) 33–39.

[40] M. Gilbert, J.-C. Sublet, A. Turner, Handbook of activation, transmutation, and radiation damage properties of the elements and of iter materials simulated using fispact-ii & tendl-2015; iter fw armour focus, Tech. rep., Tech. Rep. CCFE (2016).

[41] T. Davis, D. Healy, A. Bubeck, R. Walker, Stress concentrations around voids in three dimensions: The roots of failure, Journal of Structural Geology 102 (2017) 193–207.

[42] R. Barnes, Embrittlement of stainless steels and nickel-based alloys at high temperature induced by neutron radiation, Nature 206 (4991) (1965) 1307.

[43] E. N. Hoffman, D. W. Vinson, R. L. Sindelar, D. J. Tallman, G. Kohse, M. W. Barsoum, MAX phase carbides and nitrides: Properties for future nuclear power plant in-core applications and neutron transmutation analysis, Nuclear Engineering and Design 244 (2012) 17–24.

[44] M. A. Tunes, V. M. Vishnyakov, S. E. Donnelly, Synthesis and characterisation of high-entropy alloy thin films as candidates for coating nuclear fuel cladding alloys, Thin Solid Films 649 (2018) 115–120.

[45] C. Lu, L. Niu, N. Chen, K. Jin, T. Yang, P. Xiu, Y. Zhang, F. Gao, H. Bei, S. Shi, M.-R. He, I. M. Robertson, W. J. Weber, L. Wang, Enhancing radiation tolerance by controlling defect mobility and migration pathways in multicomponent single-phase alloys, Nature Communications 7 (2016) 13564.

List of Figures

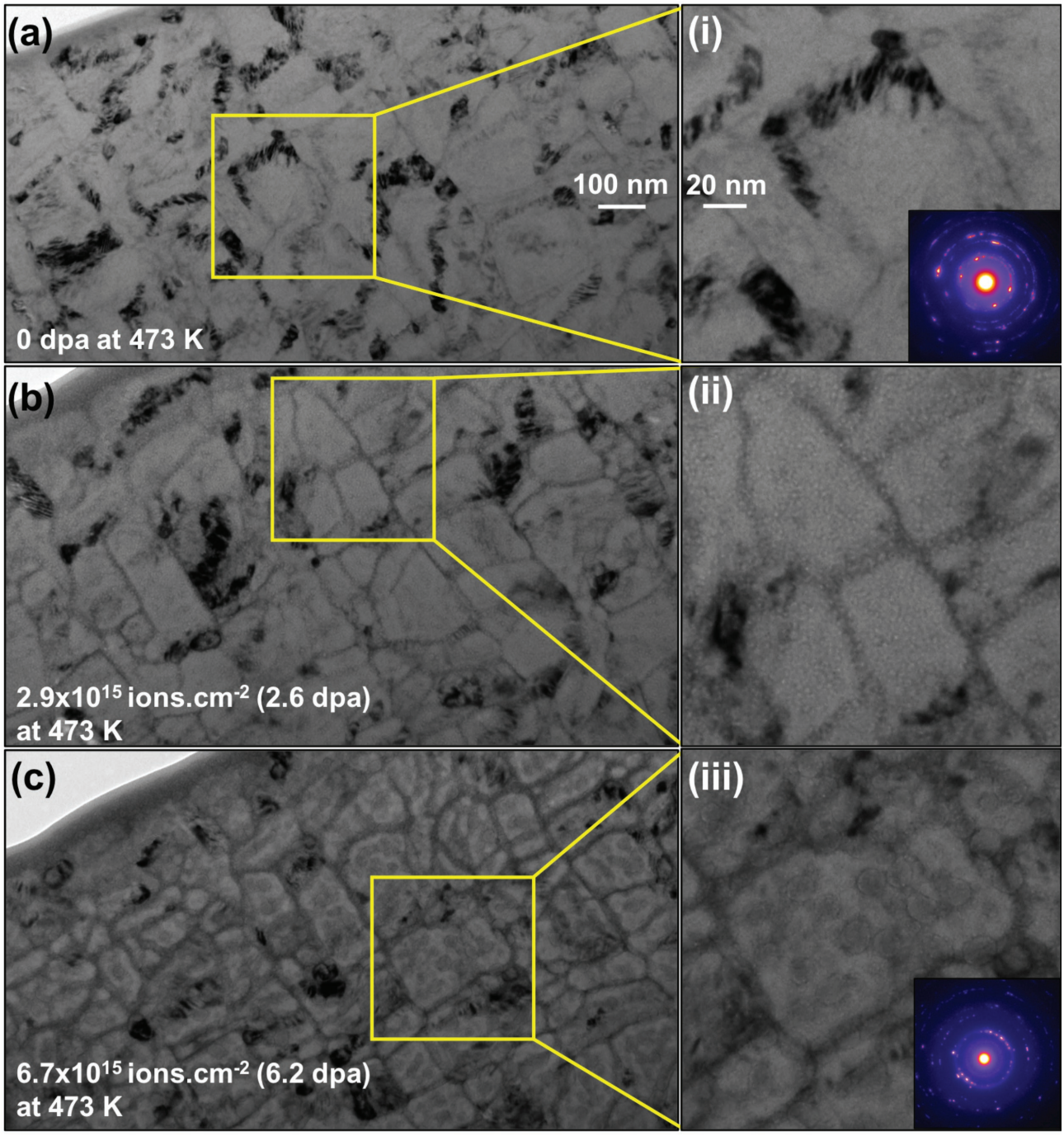

Figure 1: The microstructural evolution of the TiN microstructure under 134 keV Xe ion irradiation *in situ* in a TEM at 473 K: (a) pristine, (b) 2.9×10^{15} ions·cm^{-2} (2.6 dpa) and (c) 6.7×10^{15} ions·cm^{-2} (6.2 dpa). The outsets (i)–(iii) are micrographs of the indicated areas taken at higher magnification. Notes: all the micrographs were taken at underfocused conditions with defocus degree of 1000 nm; the scale marker in (a) also applies to (b) and (c) and the scale marker in (i) also applies to (ii) and (iii).

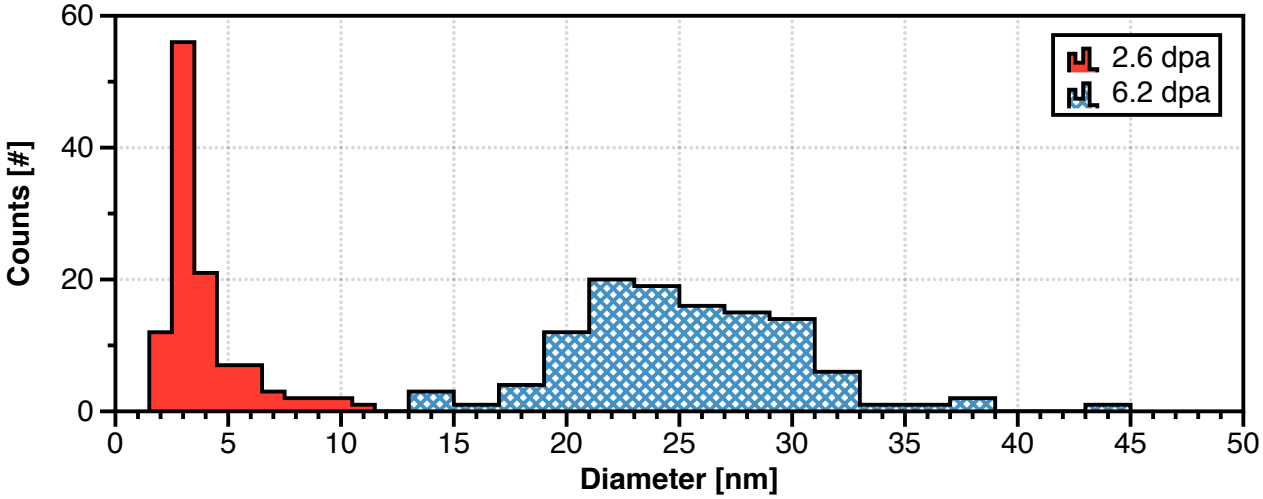

Figure 2: The diameter size distribution of Xe bubbles within the TiN.

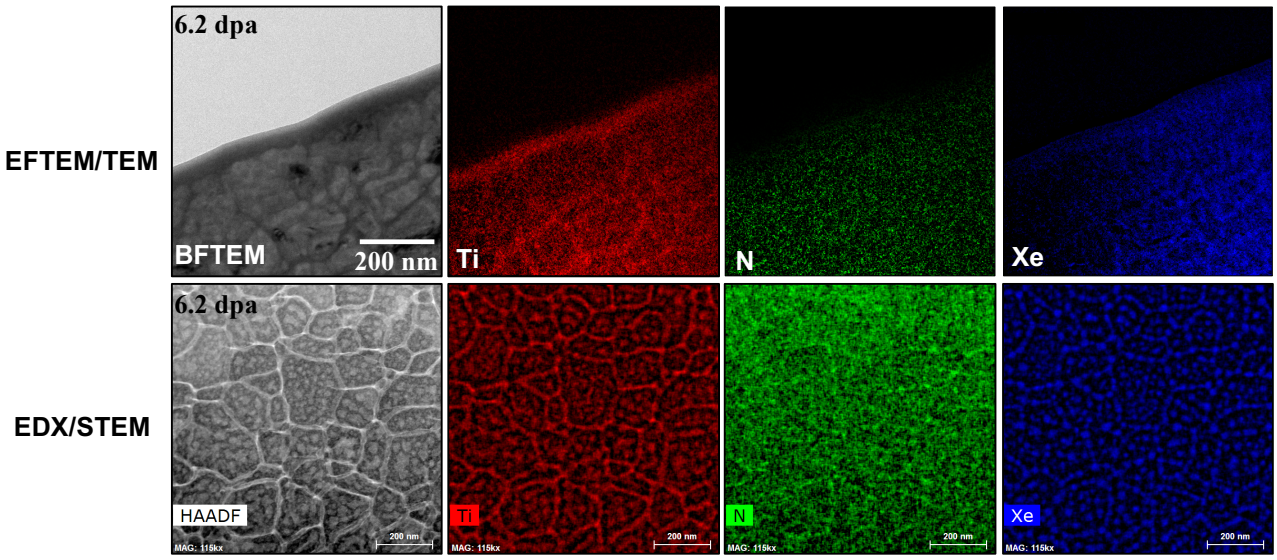

Figure 3: Post-irradiation comparison between EFTEM/TEM and EDX/STEM in the TiN at 6.2 dpa: both techniques show Ti segregation at Xe bubbles and at the grain boundaries.

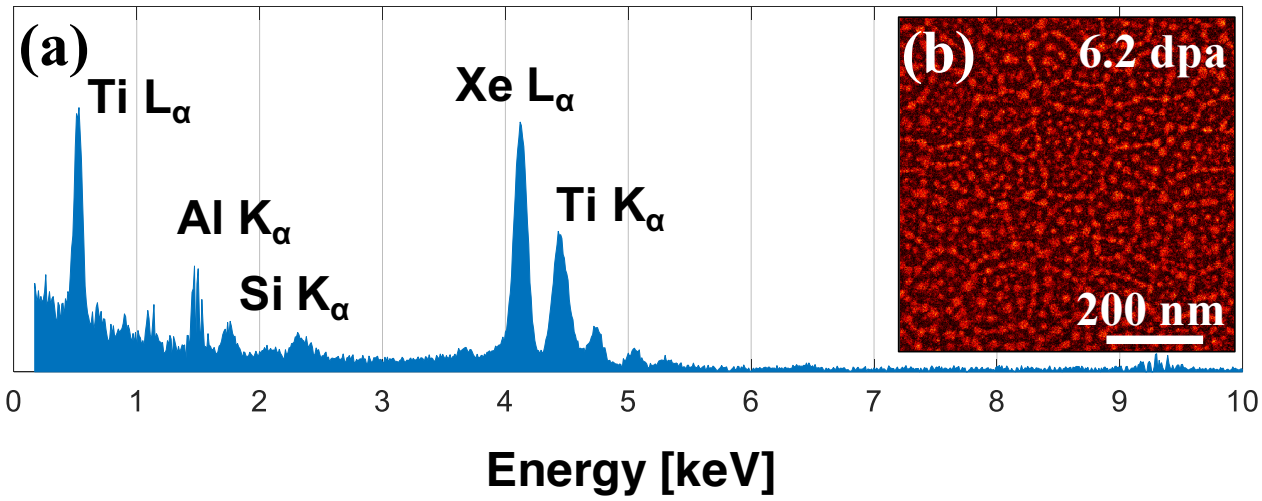

Figure 4: The multivariate statistical analysis showing the rank-3 results for (a) the EDX spectrum corresponding to the (b) spectral image (inset). The highlighted areas in the spectral image show the presence of Ti within Xe bubbles after 6.2 dpa of irradiation. The rank-1 and -2 data consisted of the matrix only and is not shown for clarification.

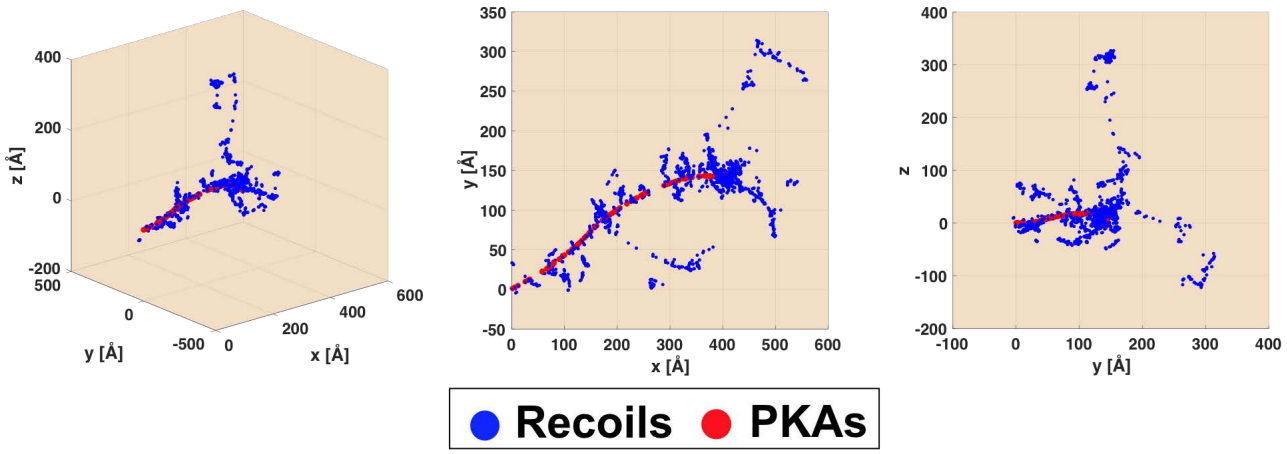

Figure 5: The cascade generated by the collision between a single Xe ion with 134 keV and the TiN thin film, taken from SRIM.

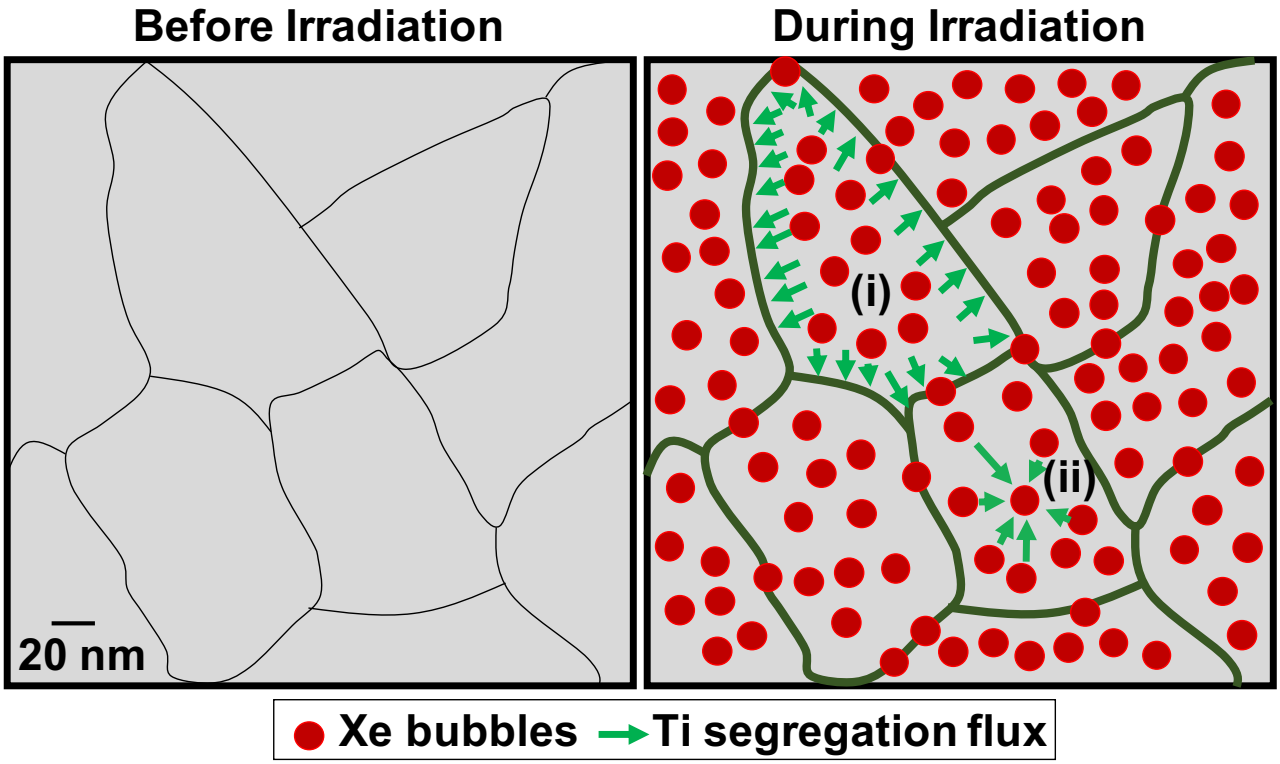

Figure 6: The two mechanisms of irradiation-induced segregation observed in this work: (i) the transgranular (isotropic) flux of Ti towards the grain boundaries upon the nucleation of Xe bubbles and (ii) the entrapment of Ti within the Xe bubbles.